Antitumor Agents

International Edition: DOI: 10.1002/anie.201913675
German Edition: DOI: 10.1002/ange.201913675

Arsenene: A Potential Therapeutic Agent for Acute Promyelocytic Leukaemia Cells by Acting on Nuclear Proteins

Xiuxiu Wang[+], *Yi Hu*[+], *Jianbin Mo*[+], *Jingyi Zhang, Zhenzhen Wang, Wei Wei, Huanlin Li, Yun Xu, Jing Ma, Jing Zhao,* Zhong Jin,* and Zijian Guo**

Dedicated to the 100th anniversary of the School of Chemistry and Chemical Engineering, Nanjing University

Abstract: *Arsenene has recently emerged as a promising new two-dimensional material for biomedical applications because of its excellent optical and electronic properties. Herein, novel 2D arsenene nanosheets were synthesized and shown to be effective against NB4 promyelocytic leukaemia (APL) cells (82 % inhibition) as well as inducing apoptosis while showing no toxicity towards normal cells. The high zeta potential, small size, and the planar structure were crucial to the toxicity of the materials. Label-free proteomic profiling analysis suggested that arsenene affected nuclear DNA replication, nucleotide excision repair, and pyrimidine metabolism pathways by downregulating the DNA polymerases POLE, POLD1, POLD2, and POLD3. Mass spectrometric studies showed that arsenene bound mainly to nuclear nucleotide acid binding proteins in NB4 cells and further cellular fluorescence studies revealed that the arsenene destroyed the nuclei. In vivo toxicity tests in mice also indicated the physiological biosafety of arsenene.*

Introduction

Two-dimensional (2D) materials have attracted increasing interest because of their wide applications in electronics, catalysis, energy storage, and biomedicine.[1] Mono-elemental 2D materials such as phosphorene, antimonene, and borophene are particularly promising because of their extraordinary physicochemical properties and outstanding biocompatibility;[2] their electronic and optical properties have resulted in them being regarded as promising anticancer therapeutics.[3] Yu and co-workers reported that 2D phosphorene could induce significant arrest of the G2/M phase in cancer cells, leading to targeted apoptotic and autophagic cell death with great selectivity.[2b] Antimonene-based photonic drug-delivery platforms initiated the application of 2D antimonene nanomaterials in cancer theranostics.[2c,4] Bismuth nanoparticles and 2D tellurium nanosheets have also been reported as efficient cancer theranostic agents for bioimaging-guided synergistic thermoradiotherapy and photodynamictherapy.[5] Other 2D nanosheets, such as germanene quantum dots, can also be used as photothermal agents for photonic cancer nanomedicine.[6] Biotite nanosheets can be engineered as intelligent theranostic platforms for imaging-guided treatment of breast cancer.[7] Arsenene is a 2D material that has recently emerged as having a layered structure similar to the buckled honeycomb structure of phosphorene. As a consequence of its suitable moderate band gap (1.66 eV), high carrier mobility, and good optical properties,[8] arsenene has commonly been applied in semiconducting devices, photocatalytic applications, nanomaterial fabrication, electrocatalysis, spintronic devices, and flexible 2D electronics.[9] In addition, arsenene is a highly efficient bifunctional material for photovoltaics and photocatalytics.[10] However, little effort has been devoted to exploring the biomedical behavior of arsenene, especially its action in cancer cells.[11]

The most popular biological application of arsenic is as arsenic trioxide, which is used to treat acute promyelocytic leukaemia (APL). As_2O_3 promotes the degradation of the oncogenic promyelocytic leukaemia protein PML-RARα that drives the growth of APL cells.[12] A recent study showed that As_2O_3 induced PML/RARA cross-linking through both the production of reactive oxygen species and direct binding.[13]

Herein, we report the synthesis of a novel arsenene nanosheet by liquid exfoliation and applied it in an anticancer study. Large quantities of the arsenene nanosheets were first prepared by direct ultrasonic exfoliation and then characterization carried out. The cellular cytotoxicity and mechanism of action towards cancer cells were then explored. The targeted proteins and cellular pathways affected by arsenene were then determined by a proteomic profiling analysis. Further imaging in NB4 cells revealed that arsenene destroyed the nucleus and deformed the organelles. LC-MS/MS-based identification of the proteins indicated that arsen-

---

[*] X. Wang,[+] Y. Hu,[+] J. Mo,[+] J. Zhang, J. Ma, J. Zhao, Z. Jin, Z. Guo
State Key Laboratory of Coordination Chemistry
Key Laboratory of Mesoscopic Chemistry of MOE
Jiangsu Key Laboratory of Advanced Organic Materials
Chemistry and Biomedicine Innovation Center (ChemBIC)
School of Chemistry and Chemical Engineering
Nanjing University, Nanjing, 210023 (China)
E-mail: jingzhao@nju.edu.cn
zhongjin@nju.edu.cn
zguo@nju.edu.cn

W. Wei, H. Li, Y. Xu
School of Life Sciences, Nanjing University
Nanjing, 210023 (China)

Z. Wang
Medical school of Nanjing University
Nanjing University
Nanjing, 210023 (China)

[+] These authors contributed equally to this work.

Supporting information and the ORCID identification number for one of the authors of this article can be found under: https://doi.org/10.1002/anie.201913675.

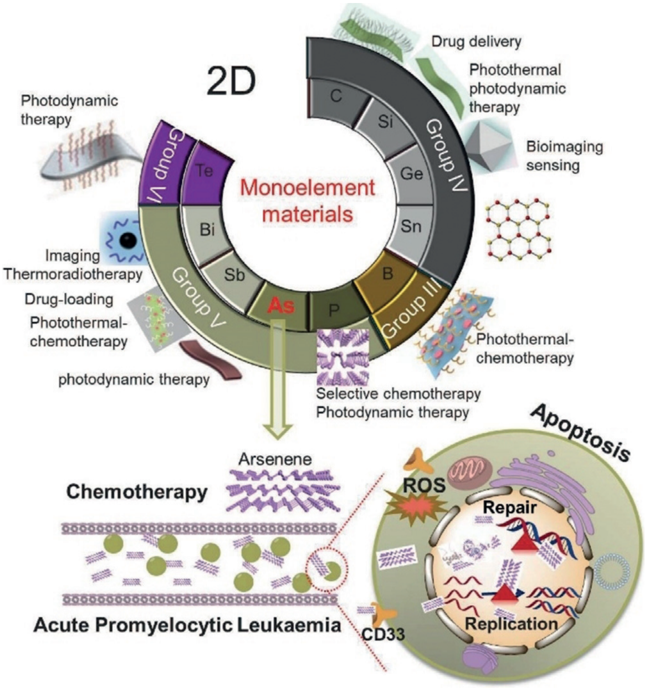

Scheme 1. An overview of the biomedical applications of 2D monoelement materials and the first investigation of arsenene in acute promyelocytic leukemia (APL) cells in this study.

ene binds mainly to RNA-binding proteins. Toxicity testing in mice was also investigated (Scheme 1).

Results and Discussion

Arsenene was synthesized by liquid exfoliation. Liquid exfoliation is commonly employed to prepare two-dimensional materials,[14] and is a simple, convenient, and low-cost method to achieve large-scale two-dimensional materials. The arsenene was prepared by sonicating gray arsenic crystals in dimethyl sulfoxide (DMSO; see the experimental section for details). The resulting samples were freeze-dried after centrifugal separation and then characterized by scanning electron microscopy (SEM). After the exfoliation process, the resulting arsenene shows a nanosheet morphology (Figure 1 b,c). The size distribution of the as-prepared arsenene nanosheets was determined by dynamic light scattering (Figure 1 d), which showed a normal distribution with a median size of 200.8 nm. Figure 1 e,f illustrate differently magnified TEM images of the as-prepared arsenene, showing they are ultrathin and confirming the successful exfoliation of arsenene. The digital photograph of the arsenene in DMSO (Figure 1 e inset) indicates the formation of a characteristic homodispersion. Figure 1 g shows typical Raman spectra of the as-prepared arsenene before and after storage in DMSO for 10 days. The two bands in the Raman spectrum have Raman shifts of 196.1 cm^{-1} and 258.5 cm^{-1}, which are in good accordance with the previously reported E_g (in-plane vibration) and A_{1g} (out-of-plane vibration) modes of arsenic, respectively.[15] A broad, weak band corresponding to amorphous arsenic at approximately 200–260 cm^{-1} can also be observed, thus indicating a slight amorphization of the arsenene after exfoliation.[16] The use of oxygen-free conditions during the exfoliation of the arsenene led to no bands corresponding to arsenic oxide being observed in the Raman spectrum. The Raman spectrum recorded after soaking arsenene for 10 days in DMSO demonstrated nearly identical bands as the freshly prepared arsenene, thus confirming the outstanding stability of arsenene in DMSO. Similarly, the Raman spectrum of arsenene dispersed in H_2O, PBS, and medium after 5 days storage was also unaffected. The crystalline arsenene partially converts into amorphous arsenene and no bands of arsenic oxide were observed in the Raman spectrum after storage (Figure S1).

To further compare the variations in the valence state of the arsenic before and after exfoliation, wide-scan X-ray photoelectron spectroscopy (XPS) characterization of the bulk arsenic precursor and freshly prepared arsenene nanosheets were performed. The XPS spectra of the bulk arsenic precursor and freshly prepared arsenene nanosheets showed no impurities (Figure S2). The XPS spectrum of bulk arsenic exhibits two bands at 42.3 eV and 41.6 eV, which are assigned to the $3d_{3/2}$ and $3d_{5/2}$ orbitals of arsenic, respectively (Figure 1 h). In addition, a weak band located at 44.6 eV was ascribed to As_2O_3, which may be attributed to air exposure. However, the XPS spectrum of the arsenene nanosheets showed only two bands with binding energies of 41.9 eV and 41.3 eV, which can also be assigned to the $3d_{3/2}$ and $3d_{5/2}$ bands of arsenic, but with a slight shift relative to bulk arsenic. The positional shifts were similar to the previously reported shear-exfoliated arsenene,[17] in which the XPS bands of the As 3d bands were red-shifted after the exfoliation process.

X-ray diffraction (XRD) characterization was performed to verify the crystallinity and high purity of the as-prepared arsenene. The XRD patterns are in good agreement with rhombohedral phase arsenic (JCPDS PDF card No. 05-0632; Figure 1 j). The corresponding SAED patterns and high-resolution TEM characterizations showed the as-prepared arsenene contained both crystalline and amorphous features (Figure 1 k). AFM characterizations were then performed to investigate the topography and height of the exfoliated arsenene. The AFM image and corresponding height profiles showed well-dispersed arsenene on the mica substrate with a thickness of dozens of nanometers (Figure S3).

To better quantify the chemical features of the arsenene nanosheets, electrochemical measurements of the exfoliated pnictogen 2D materials were then performed. Pioneered by Pumera and co-workers, the electrochemical properties of layered materials were found to be crucial to the properties and functions of the materials.[18] The cyclic voltammograms of GC electrodes modified with arsenene, antimonene, and bismuthene materials with an inner-sphere redox ferro-/ferricyanide probe were recorded (Figure 1 l and see also Figure S4). The potential difference between the oxidation and reduction (ΔEp) of each cyclic voltammogram was calculated. The intrinsic quantitatively electrochemical potential of exfoliated arsenene, antimonene, and bismuthene were also investigated in phosphate-buffered saline (PBS, pH 7.2), which is consistent with the environments of living cells. The electrochemical potentials of arsenic, antimony, and

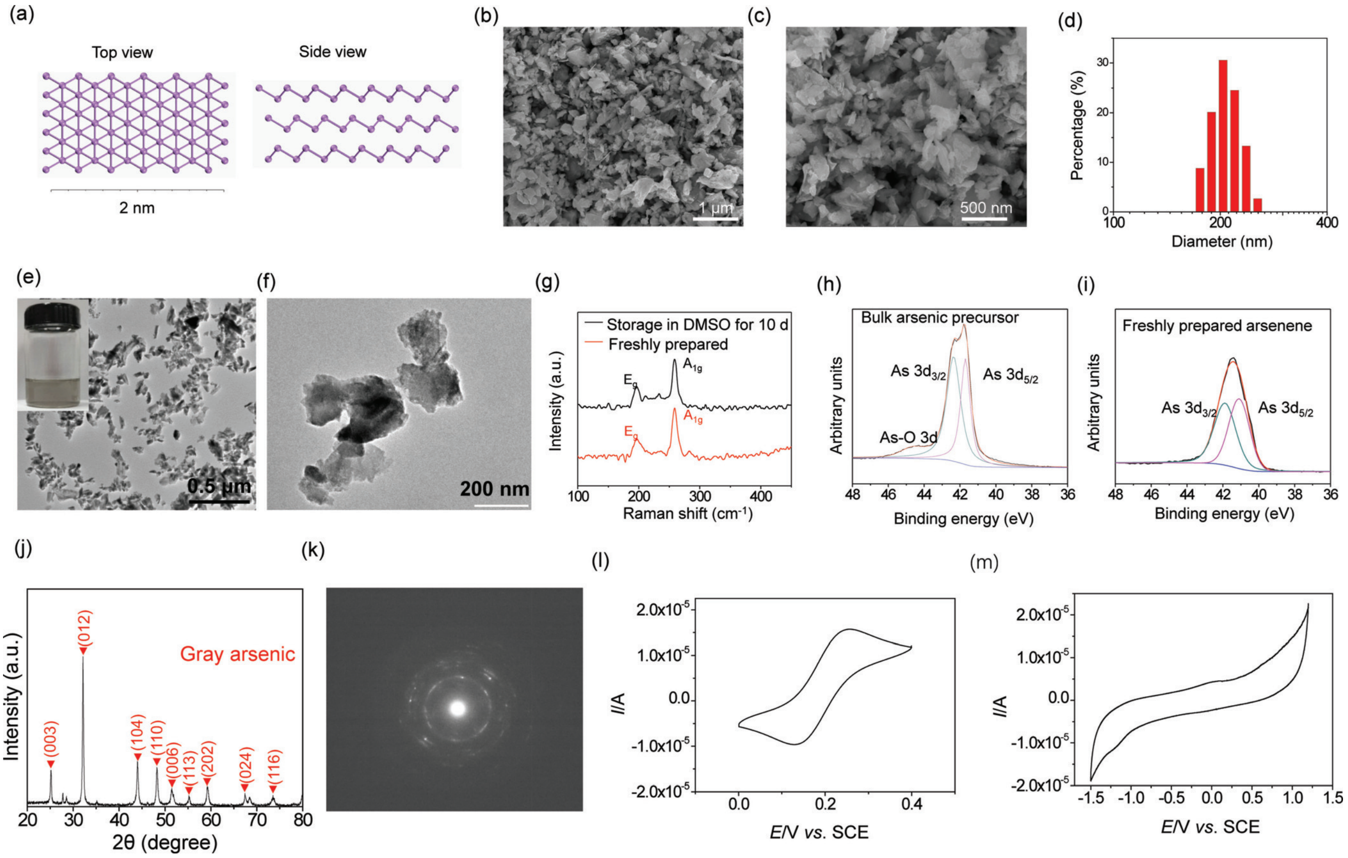

Figure 1. Characterization of arsenene. a) Structures of monolayer arsenene, top and side views. b, c) SEM images of as-synthesized arsenene nanosheets. d) Size distribution of the arsenene nanosheets. e, f) TEM images of arsenene nanosheets at different magnifications; the inset in (e) shows a digital photo of the arsenene nanosheets dispersed in DMSO. g) Raman spectra of freshly prepared arsenene (red line) and after storage in DMSO for 10 days (black line). h, i) XPS spectra of h) the bulk arsenic precursor and i) freshly prepared arsenene nanosheets. j) Characterization of the arsenene nanosheets by XRD. k) SAED patterns of arsenene nanosheets. l) Cyclic voltammograms (CVs) obtained with a 1.0 mm ferro-/ferricyanide $[Fe(CN)_6]^{3-}/[Fe(CN)_6]^{4-}$ redox probe in 0.1 м KCl using a GC electrode modified with arsenene. m) Cyclic voltammograms of arsenene in 0.1 м PBS at pH 7.2 and a scan rate of 100 mV s^{-1}.

bismuth in the three-electron redox process are −0.55, −0.92, and −0.69 V, respectively (Figure 1 m and see also Figure S5).

Next, we determined the cytotoxicity of arsenene nanosheets towards five cancer cell lines (A2780 human ovarian cancer cells, A549 human lung cancer cells, HeLa human cervical cancer cells, MCF-7 human breast cancer cells, and NB4 acute promyelocytic leukaemia cells) and one human normal liver cell line (L-02) using a CCK8 cell viability assay. Arsenene exhibited significant cell inhibition towards the NB4 cancer cells with an inhibition of 82 % after treatment with 1.2 μg mL^{-1} arsenene, while no cell inhibition was detected in the normal L-02 cells, thus indicating the significant selectivity of arsenene (Figure 2 a). Fluorescent microscopy images obtained after co-staining of the cells with calcein AM (live cells, green fluorescence) and propidium iodide (PI; dead cells, red fluorescence) after treatment with arsenene provided similar results, thus confirming a significant inhibition of the NB4 cells by arsenene (Figure 2 b).

We then investigated the cytotoxicity caused by arsenene in terms of its electrochemical potential and structure. The exfoliated arsenene has a planar structure and a size of 200.8 nm, so a comparison was made with a different-sized arsenene (749.3 nm) and a bulk material. First, we examined the effect of the zeta potential on the cell cytotoxicity. The zeta potential of the 200.8 nm sized arsenene was −17.8 mV, while those of the 749.3 nm sized arsenene and the bulk material were −9.03 mV and −4.69 mV, respectively. The arsenic uptake from the larger arsenene and bulk materials was less in the same four cancer cells (MCF-7, A549, A2780, NB4) and one normal cell (L-02) than from the 200.8 nm sized arsenene, and no apparent growth inhibition was observed in the five cell lines (Figures S6 and S7).

To further confirm the effect of the zeta potential, we compared arsenene with other 2D nanosheets: antimonene, black phosphorus (BP), and bismuthene. BP displayed a potential of −18.0 mV, similar to that of arsenene (−17.8 mV), while antimonene and bismuthene possessed lower zeta potentials (−1.78 mV and 0.921 mV, respectively). The cell cytotoxicity study indicated that the antimonene and bismuthene nanosheets resulted in no growth inhibition, while BP with a similar potential led to an approximately 30 % inhibition. The higher potential was reported to result in a better dispersion of materials,[19] which could promote cell uptake. All these results indicated that the higher zeta potential, the smaller size, and the planar structure were crucial to the toxicity of the arsenic materials (Figure 2 c,d).

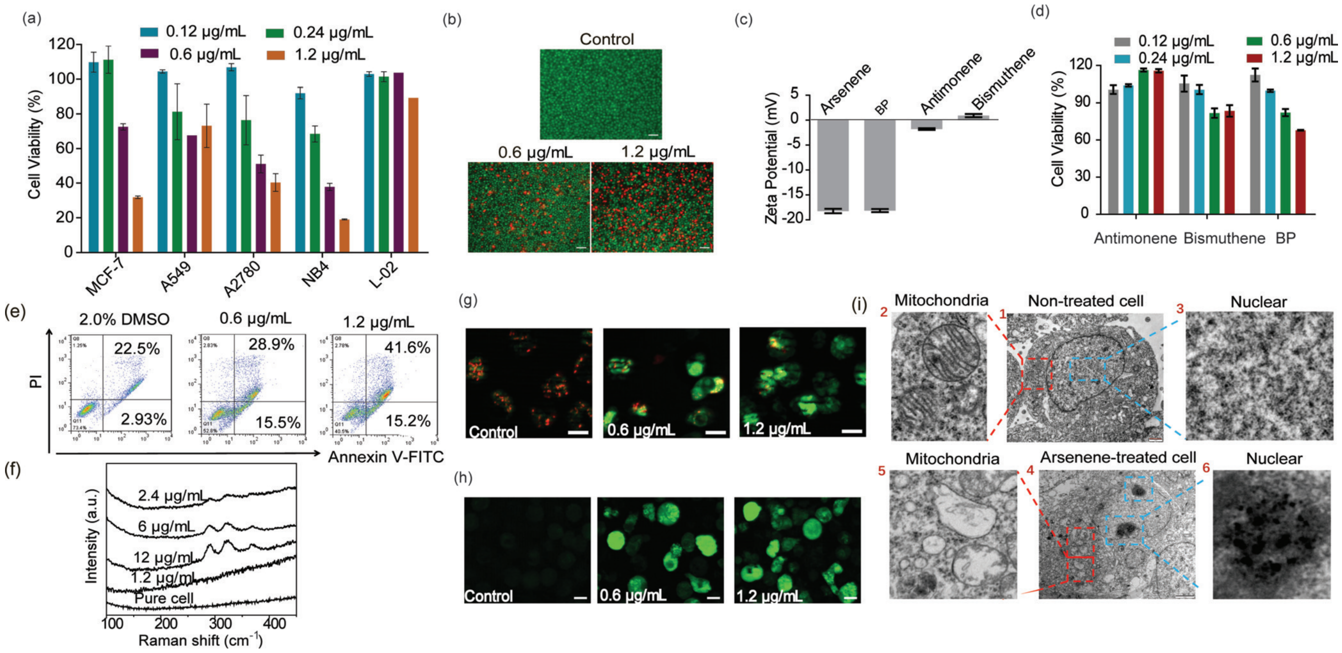

Figure 2. Anticancer activity of arsenene nanosheets. a) Cell viability of A549 cells, A2780 cells, HeLa cells, MCF-7 cells, NB4 cells, and L-02 cells treated with 0.12, 0.24, 0.6, 1.2, and 2.4 μg mL^{-1} arsenene nanosheets. The values are expressed as the mean ± standard deviation (± SD) of triplicate measurements. b) Corresponding laser scanning fluorescence microscopy of NB4 cells stained with calcein AM (live cells, green fluorescence) and PI (dead cells, red fluorescence); scale bars: 50 μm. c) Zeta potential of the arsenene nanosheets and the 2D materials BP, antimonene, and bismuthene. d) Cell viability of A549 cells, A2780 cells, HeLa cells, MCF-7 cells, NB4 cells, and L-02 cells treated with 0.12, 0.24, 0.6, 1.2, and 2.4 μg mL^{-1} BP materials, antimonene, and bismuthene. e) Apoptosis detected by flow cytometry in arsenene-treated NB4 cells through annexin V-FITC/PI staining. Early apoptotic cells are shown in the lower right quadrant, and late apoptotic cells are shown in the upper right quadrant. g) Mitochondrial membrane potential detected by fluorescence microscopy after JC-1 staining. Red represents hyperpolarization and green represents depolarization of the mitochondrial membrane potential. f) Raman spectra of As in NB4 cells treated with different concentrations of arsenene. h) Intracellular ROS production in arsenene-treated NB4 cells detected by fluorescence microscopy after DCFH-DA staining; scale bars: 10 μm. i) TEM images of arsenene-treated NB4 cells. Images 1 and 4 are whole-cell TEM images of untreated and arsenene-treated NB4 cells, respectively; images 2 and 3, and 5 and 6 are enlarged images of 1 and 4, respectively (red dotted line, mitochondria; blue dotted line, condensed chromatin). Values are expressed as the mean ± SD of triplicate measurements.

To explore the mechanism of the inhibition, an apoptotic study was conducted, and both early and late apoptotic cells were detected by flow cytometry: 41.6 % of the cells suffered from late apoptosis (Figure 2 e). The change in the mitochondrial transmembrane potential (Δψ), one of the earliest events in the process of apoptosis, was examined to confirm apoptosis occurred after arsenene treatment. 5,5′,6,6′-Tetrachloro-1,1′,3,3′-tetraethylbenzimidazolcarbocyanine iodide (JC-1), a cationic lipid fluorescent dye, was utilized as an indicator to detect the mitochondrial membrane potential (MMP). The results indicated a depolarization of the mitochondria, an early signal of apoptosis, which further confirmed the induction of apoptosis by arsenene (Figure 2 g). Furthermore, the Raman spectrum of NB4 cells treated with arsenene indicated the presence of the oxidative form of the arsenic nanosheets (Figure 2 f). The Raman intensity clearly decreased until the concentration of arsenene had finally vanished. The pure cell showed no similar Raman bands, thus confirming that the three bands originated from arsenene or its derivative. The two characteristic bands of arsenene disappeared, and three new Raman bands emerged in the Raman spectrum of arsenene after cell experiments. The three Raman bands were centered at 290, 322, and 368 cm^{-1}. The band located at 368 cm^{-1} is consistent with the A_{1g} mode of arsenolite (As_2O_3).[20] Based on a previous report, the bands with Raman shifts of 290 cm^{-1} and 322 cm^{-1} can be explained as combination bands, which can be calculated by the difference between the T_{2g} and E_g modes.[20]

Considering the possible oxidized form of arsenene in NB4 cells and the reactive oxygen species (ROS) produced by arsenic trioxide,[13b] the presence of ROS in arsenene-treated NB4 cells was investigated by staining with a cell-permeable fluorescent dye (dichlorofluorescein, DCF). A strong green fluorescence was observed in cells after treatment with arsenene, which indicates the generation of ROS inside the cells (Figure 2 h and see also Figure S8). The production of ROS has been recognized as a major toxicological property of nanomaterials.[21] The significantly increased level of ROS induced by arsenene might contribute to the cytotoxicity. Morphological changes in the arsenene-treated cells were observed by transmission electron microscopy (TEM). TEM images of arsenene-treated NB4 cells displayed a vanishing and weakened mitochondrial ridge. Condensed chromatin in the nucleus was also observed, which further verified the apoptosis process induced by arsenene (Figure 2 i). Together, the overproduction of ROS and the depolarization of the MMP might synergistically contribute to apoptosis of the NB4 cells, thereby leading to inhibition of the NB4 cells.

To further explore the mechanism of action of arsenene in cells, label-free quantitative proteomics profiling was conducted in the NB4 cells. Differentially expressed proteins were screened according to the standard of a 1.5-fold change in expression. This led to 61 proteins being identified as upregulated, while 99 proteins were identified as downregulated (Figure 3 b and Table S1). Among these proteins, 42.5 % are in the nucleus, 28.75 % are in the cytoplasm, and 7.5 % are in mitochondria (Figure 3 a). From the volcano map, the most downregulated protein was thioredoxin-like protein 1 (TXNL1), which generates disulfide oxidoreductase activity and preserves cell redox homeostasis by acting on thioredoxin with a redox potential of approximately −250 mV.[22] Thus, TXNL1 might be one of the main targets of arsenene. The decreased expression of TXNL1 in arsenene-treated cells probably affects the redox homeostasis of whole cells (Figure 3b). A bioinformatics analysis of all the differentially expressed proteins using KEGG (Kyoto Encyclopedia of Genes and Genomes) pathway screening showed that the base excision repair pathway, pyrimidine metabolism, and DNA replication pathways were apparently affected (Figure 3c and Table S2). There were four common proteins in the three screened pathways: DNA polymerase epsilon catalytic subunit A (POLE), DNA polymerase delta catalytic subunit (POLD1), DNA polymerase delta subunit 2 (POLD2), and DNA polymerase delta subunit 3 (POLD3) (Figure 3 d). The decrease in these proteins indicated that arsenene reduced the replication ability of whole-cell DNA and weakened cellular base excision repair processes and pyrimidine metabolism processes in the NB4 cells.

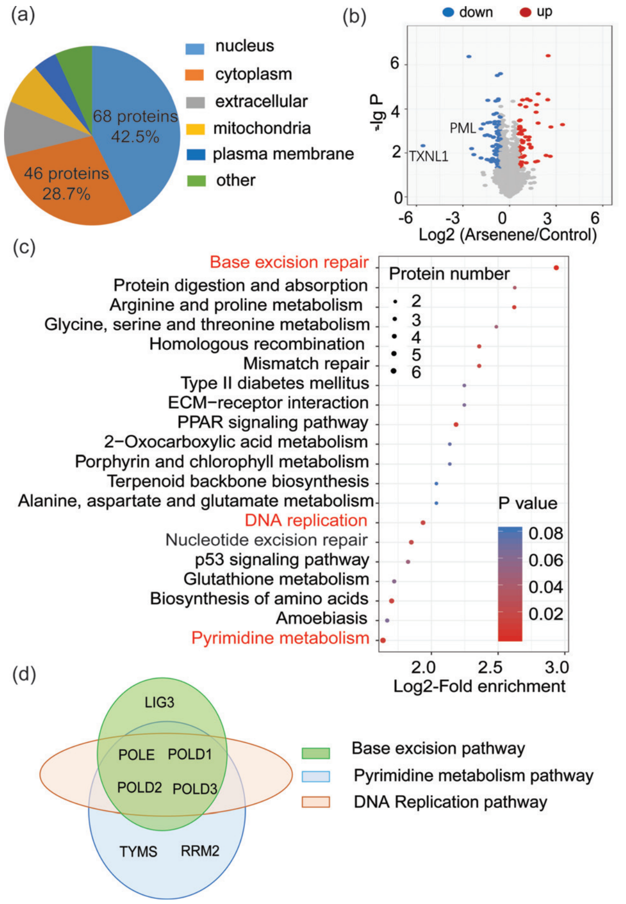

Figure 3. Proteomics analysis of arsenene-treated cells compared with control cells. a) Subcellular localization chart of differentially expressed proteins. b) Volcano plot of differentially expressed proteins. Downregulated proteins are shown in blue, upregulated proteins in red, and unchanged proteins in gray. c) KEGG pathway enrichment bubble plot of differentially expressed proteins in arsenene-treated NB4 cells, compared with untreated groups. d) The common proteins (POLE, POLD1, POLD2, and POLD3) in the screened pathways.

Next, TXNL1 and three different DNA polymerase proteins, POLD1, POLD3, and POLE, in the screened pathways were expressed and verified by western blot analysis. The western blot results indicated that all the detected nuclear proteins were downregulated after treatment with arsenene for 12 h and 24 h (Figure 4 a). The mode of action of the current clinical drug As_2O_3 for the treatment of APL disease is to bind to the nuclear zinc finger protein PML, thereby leading to apoptosis of the NB4 cells, and inhibiting the proliferation of cells. We found that arsenene can also inhibit the expression of the PML protein, but no binding was detected by western blot of PML in arsenene-binding proteins (Figure 4 a and see Figure S15).

Arsenene-binding proteins were separated by centrifugation from the cell protein mixture to determine the type of proteins that bind to arsenene. LC-MS/MS was used to identify the bound proteins. The mass spectrometric results showed that the arsenene-bound proteins were mainly nucleotide acid binding proteins (197 proteins) and involved in gene expression processes according to Gene Ontology (GO) analysis, which is distinct from As_2O_3[12] (Figure 4 e). This difference can be explained from the distinct structure of the arsenic nanosheets compared with the solution state of As_2O_3. It is not surprising to observe different modes of action between a monoelement material and arsenic oxide species. Of the identified binding proteins, 106 proteins were located in the nucleus, such as non-histone chromosomal protein HMG-17 (HMGN2) and splicing factor 3B subunit 1 (SF3B1; Table S3). Considering that the bound nuclear proteins may be affected by arsenene, a morphological image of the arsenene-treated nucleus after Hoechst 33342 staining was recorded. The nuclear cellular imaging revealed that arsenene destroyed the nuclei and formed nuclear fragments, which is consistent with the results of the differential protein concentration in the nucleus in the above proteomic analysis (Figure 4 b and Figure S10).

In addition, the cellular images of organelles in arsenene-treated NB4 cells displayed damaged cell membranes, lysosomes, mitochondria, and endoplasmic reticulum, which resulted in polycondensation in the cells (Figure 4 d and Figures S11–S14). The surface protein CD33, a 67 kDa glycoprotein, is involved in cell adhesion or communication. CD33 is expressed on leukaemia cells in more than 90 % of patients[23] and expressed in 99.7 % of NB4 cells.[24] Immunofluorescence detection showed that the CD33 expression of the NB4 cells was greatly downregulated after the action of arsenene, thus indicating that arsenene could also eliminate NB4 cells by inhibiting the cell surface recognition by glycoprotein CD33 (Figure 4 c).

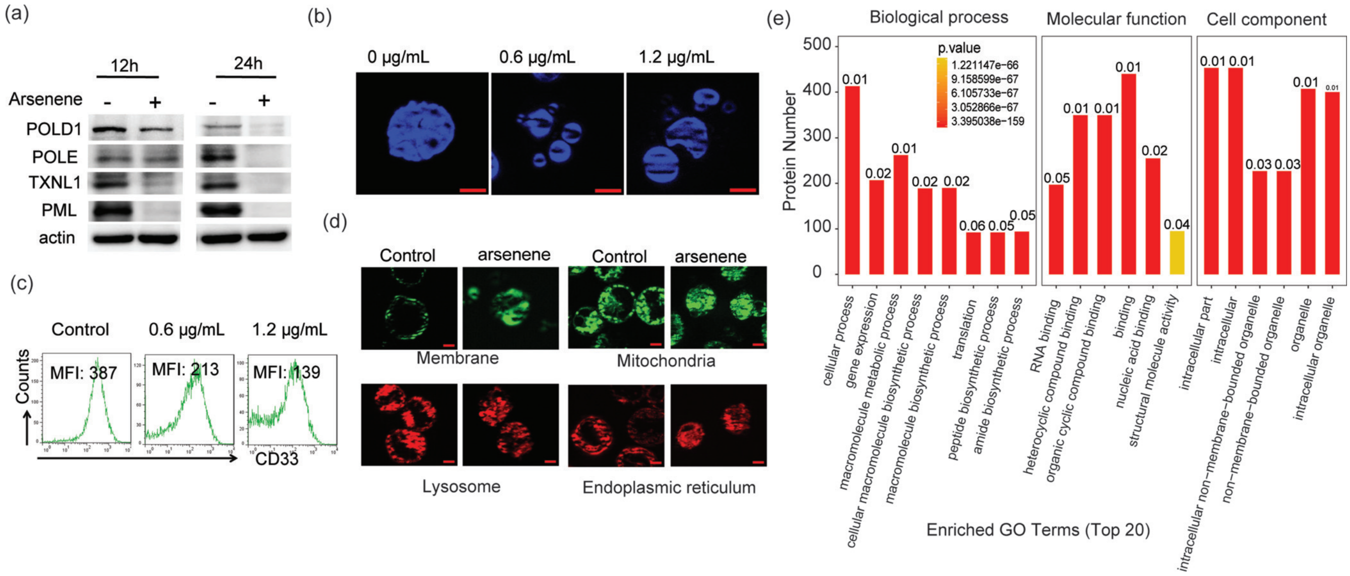

Figure 4. Verification of arsenene action on cellular proteins and arsenene-binding proteins in NB4 cells. a) Western blot of differentially expressed nuclear proteins (TXNL1, POLD1, POLD3, POLE, and PML) in arsenene-treated NB4 cells, compared with untreated NB4 cells. b) Nuclear images in arsenene-treated cells and untreated NB4 cells. Scale bar: 5 μm. c) Immunofluorescence detection of CD33 in arsenene-treated NB4 cells by flow cytometry. d) Images of organelles affected by different concentrations of arsenene, including the membrane, lysosome, mitochondria, and endoplasmic reticulum using membrane tracker green, lysosome tracker red, mitochondrial tracker green, and endoplasmic reticulum tracker red. Scale bar: 5 μm. e) GO analysis of arsenene-binding proteins in terms of biological processes, molecular functions, and cellular components.

A toxicity test in mice was then conducted to assess the potential of the 2D nanosheet materials in vivo. Based on the above cellular cytotoxicity of arsenene to NB4 cells and nontoxicity towards normal L-02 cells, arsenene concentrations of 0.375 $\mathrm{mg\,kg^{-1}}$, 0.75 $\mathrm{mg\,kg^{-1}}$, 1.5 $\mathrm{mg\,kg^{-1}}$ and 3 $\mathrm{mg\,kg^{-1}}$ were injected into mice. Haematological and blood biochemical analysis of the liver/kidney function were performed after 1 day, 7 days, and 14 days. For the haematological analysis, we detected standard hematology markers, white blood cells (WBCs), red blood cells (RBCs), hemoglobin (HGB), hematocrit (HCT), mean corpuscular volume (MCV), mean corpuscular hemoglobin (MCH), mean corpuscular hemoglobin concentration (MCHC), and platelets (PLTs) in the arsenene-treated mice and compared them with those from untreated mice.[25] The WBC, RBC, HGB, HCT, MCV, MCH, MCHC, and PLT values did not show any meaningful differences from those of the untreated mice ($P > 0.05$), thus indicating no apparent infection and inflammation caused by arsenene treatment (Figure 5a and see Figure S17). Biochemical analysis of the blood was then carried out, including aspartate transaminase (AST), alanine transaminase (ALT), blood urea nitrogen (BUN), and lactate dehydrogenase (LDH). Compared with untreated mice, no apparent difference can be observed from mice treated with arsenene (Figure 5b and S18). Similar to alanine transaminase, aspartate transaminase is related to the liver/kidney function.[25] These two insignificant changes reveal the non-hepatic and non-kidney toxicity of arsenene in mice. Furthermore, the weights of the mice did not significantly change after treatment with arsenene for 20 days (Figure 5c).

A hemolysis test of the arsenene nanosheets with whole blood for 8 h showed the hemolysis rate was approximately close to 0%. This demonstrated that arsenene nanosheets were biocompatible with blood in vivo (Figure 5d and see Figure S16). The biodistribution of arsenene is critical for in vivo treatment. After being injected with 120 $\mathrm{\mu g\,mL^{-1}}$ arsenene for 24 h, the mice were then scarified, and the organs (liver, heart, lung, spleen, and kidney) were tested by inductively coupled plasma mass spectrometry (ICP-MS). The arsenene materials were found to be concentrated in the liver and kidney (Figure 5e). After treatment for 7 days, the pathological changes in the liver, spleen, lung, heart, and kidney were investigated by immunohistochemistry, with staining by haematoxylin and eosin (H&E). No apparent toxic effects to the liver, spleen, lung, heart, or kidney were observed (Figure 5f and see Figure S19). These results suggested that arsenene may potentially be a biosafe material with potential application for the treatment of the APL disease.

Conclusion

In this study, we focused on the crucial role of 2D arsenene nanosheets in biomedical applications. Arsenene nanosheets were synthesized by liquid exfoliation and characterized by SEM, TEM, SEAD imaging, Raman spectroscopy, XPS, and XRD. Their biochemical performance was also investigated. Arsenene nanosheets (200.8 nm and planar structure) displayed potent antiproliferative activity against a variety of cancer cells, especially NB4 acute promyelocytic leukaemia cells, but are nontoxic to normal cells. The higher zeta potential, the smaller size, and the planar structure were crucial to the toxicity of the arsenic materials.

The mechanistic study in the NB4 cells revealed that arsenene can induce the production of ROS and the

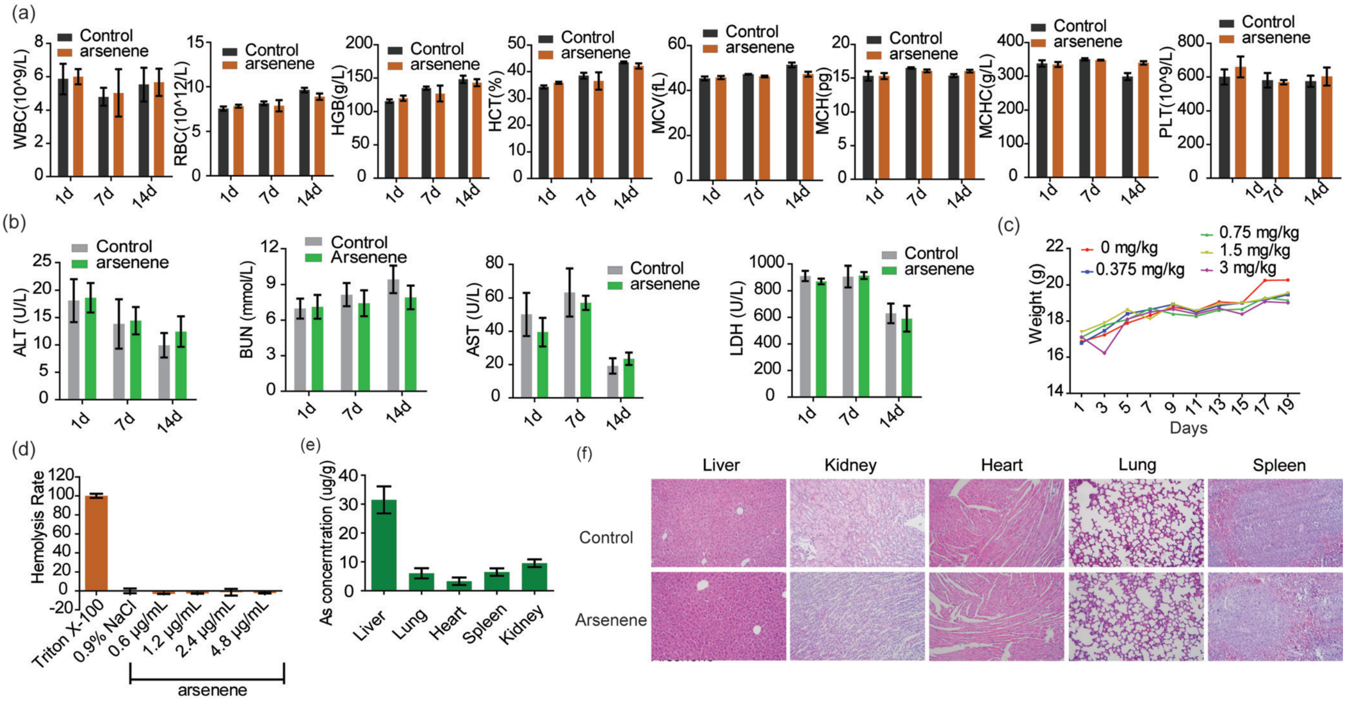

Figure 5. Toxicity test of arsenene in vivo. a) Haematological data of the mice injected with arsenene (0.75 mg kg^{-1}) at 1, 7, and 14 days post-injection. Haematological data included determination of the white blood cells, red blood cells, haemoglobin, mean corpuscular volume, mean corpuscular haemoglobin, mean corpuscular haemoglobin concentration, platelets, and haematocrit. b) Biochemical analysis of the blood of mice 1, 7 and 14 days post-injection with arsenene (0.75 mg kg^{-1}). Blood biochemical data included determination of aminotransferase, aminotransferase, blood urea nitrogen, and lactate dehydrogenase. c) The body weights of mice injected with arsenene (0.375, 0.75, 1.5, and 3 mg kg^{-1}) over 20 days. d) Hemolysis analysis of whole blood treated with arsenene nanosheets for 8 hours. e) In vivo biodistribution of arsenene in organs of mice. Values are expressed as the means ± SD of triplicate measurements. f) Haematoxylin and eosin (H&E) staining of the liver, spleen, kidney, heart, and lung of arsenene-treated mice 14 days post-injection.

depolarization of mitochondrial membrane potentials, leading to apoptosis of the NB4 cells. Quantitative proteomics studies of label-free proteins suggested that arsenene mainly affected the nuclear proteins in the NB4 cells and targeted the nuclear protein TXNL1. Thus, a decrease in TXNL1 might break the redox homeostasis in cells. Further bioinformatics analysis of the KEGG pathways indicated that arsenene mainly acted on the pyrimidine metabolism, DNA replication, and nucleotide excision repair pathways. The common nuclear proteins (POLD1, POLD3, and POLE) in these three screened pathways were all downregulated. Further cellular imaging revealed that arsenene destroyed nuclei and resulted in the formation of nuclear fragments. These morphological variations then led to the entire organelle being exposed to the cytoplasm and infection of the entire cell. Mass spectrometric studies showed that the bound proteins of arsenene in the NB4 cells were mainly 106 nuclear nucleotide acid binding proteins (such as HMGN2 and SF3B1). In addition, arsenene can also destroy CD33, thereby reducing cellular recognition. According to the in vivo toxicity testing in mice, arsenene is a biosafe material. This study suggests that arsenene might serve as a potentially biosafe material for treatment of APL disease and has provided the first insight into the use of 2D arsenene nanosheets in biomedical applications.

Acknowledgements

This work was supported by the National Natural Science Foundation of China (21622103, 21671099, 91753121, 21872069, 51761135104, 21573108), Shenzhen Basic Research Program (JCYJ20170413150538897, JCYJ20180508182240106), National Key R&D Program of China (2017YFA0208200, 2016YFB0700600, 2015CB659300), Natural Science Foundation of Jiangsu Province (BK20180008), and the Fundamental Research Funds for the Central Universities of China. We thank the Shanghai Applied Protein Technology Co., Ltd., and PTM BioLabs, Inc. for technological assistance.

Conflict of interest

The authors declare no conflict of interest.

Keywords: antitumor agents · apoptosis · arsenene · nuclear proteins · proteomics

How to cite: *Angew. Chem. Int. Ed.* **2020**, *59*, 5151–5158
Angew. Chem. **2020**, *132*, 5189–5196

[1] a) Y. B. Zhang, Y. W. Tan, H. L. Stormer, P. Kim, *Nature* **2005**, *438*, 201 – 204; b) Y. F. Sun, S. Gao, F. C. Lei, Y. Xie, *Chem. Soc. Rev.* **2015**, *44*, 623 – 636; c) F. Bonaccorso, L. Colombo, G. H. Yu, M. Stoller, V. Tozzini, A. C. Ferrari, R. S. Ruoff, V. Pellegrini, *Science* **2015**, *347*, 1246501; d) Y. Chen, C. Tan, H. Zhang, L. Wang, *Chem. Soc. Rev.* **2015**, *44*, 2681 – 2701.

[2] a) J. Mo, Q. Xie, W. Wei, J. Zhao, *Nat. Commun.* **2018**, *9*, 2480; b) W. Zhou, T. Pan, H. Cui, Z. Zhao, P. K. Chu, X. F. Yu, *Angew. Chem. Int. Ed.* **2019**, *58*, 769 – 774; *Angew. Chem.* **2019**, *131*, 779 – 784; c) W. Tao, X. Ji, X. Zhu, L. Li, J. Wang, Y. Zhang, P. E. Saw, W. Li, N. Kong, M. A. Islam, T. Gan, X. Zeng, H. Zhang, M. Mahmoudi, G. J. Tearney, O. C. Farokhzad, *Adv. Mater.* **2018**, *30*, 1802061; d) X. Ji, N. Kong, J. Wang, W. Li, Y. Xiao, S. T. Gan, Y. Zhang, Y. Li, X. Song, Q. Xiong, S. Shi, Z. Li, W. Tao, H. Zhang, L. Mei, J. Shi, *Adv. Mater.* **2018**, 1803031.

[3] W. Tao, N. Kong, X. Ji, Y. Zhang, A. Sharma, J. Ouyang, B. Qi, J. Wang, N. Xie, C. Kang, H. Zhang, O. C. Farokhzad, J. S. Kim, *Chem. Soc. Rev.* **2019**, *48*, 2891 – 2912.

[4] a) W. Tao, X. Y. Ji, X. D. Xu, M. A. Islam, Z. J. Li, S. Chen, P. E. Saw, H. Zhang, Z. Bharwani, Z. L. Guo, J. J. Shi, O. C. Farokhzad, *Angew. Chem. Int. Ed.* **2017**, *56*, 11896 – 11900; *Angew. Chem.* **2017**, *129*, 12058 – 12062; b) G. H. Lu, C. L. Lv, W. E. Bao, F. Li, F. Zhang, L. J. Zhang, S. Wang, X. Y. Gao, D. X. Zhao, W. Wei, H. Y. Xie, *Chem. Sci.* **2019**, *10*, 4847 – 4853.

[5] a) X. Yu, A. Li, C. Zhao, K. Yang, X. Chen, W. Li, *ACS Nano* **2017**, *11*, 3990 – 4001; b) Y. Lin, Y. Wu, R. Wang, G. Tao, P. F. Luo, X. Lin, G. Huang, J. Li, H. H. Yang, *Chem. Commun.* **2018**, *54*, 8579 – 8582.

[6] J. Ouyang, C. Feng, X. Y. Ji, L. Li, H. K. Gutti, N. Y. Kim, D. Artzi, A. Xie, N. Kong, Y. N. Liu, G. J. Tearney, X. B. Sui, W. Tao, O. C. Farokhzad, *Angew. Chem. Int. Ed.* **2019**, *58*, 13405 – 13410; *Angew. Chem.* **2019**, *131*, 13539 – 13544.

[7] X. Y. Ji, Y. Kang, J. Ouyang, Y. H. Chen, D. Artzi, X. B. Zeng, Y. L. Xiao, C. Feng, B. W. Qi, N. Y. Kim, P. E. Saw, N. Kong, O. C. Farokhzad, W. Tao, *Adv. Sci.* **2019**, *6*, 1901211.

[8] a) S. L. Zhang, M. Q. Xie, F. Y. Li, Z. Yan, Y. F. Li, E. J. Kan, W. Liu, Z. F. Chen, H. B. Zeng, *Angew. Chem. Int. Ed.* **2016**, *55*, 1666 – 1669; *Angew. Chem.* **2016**, *128*, 1698 – 1701; b) D. Kecik, E. Durgun, S. Ciraci, *Phys. Rev. B* **2016**, *94*, 205409.

[9] a) Z. Y. Zhang, J. F. Xie, D. Z. Yang, Y. H. Wang, M. S. Si, D. S. Xue, *Appl. Phys. Express* **2015**, *8*, 055201; b) F. Ersan, E. Akturk, S. Ciraci, *J. Phys. Chem. C* **2016**, *120*, 14345 – 14355; c) H. S. Tsai, S. W. Wang, C. H. Hsiao, C. W. Chen, H. Ouyang, Y. L. Chueh, H. C. Kuo, J. H. Liang, *Chem. Mater.* **2016**, *28*, 425 – 429; d) H. C. Tao, Y. A. Gao, N. Talreja, F. Guo, J. Texter, C. Yan, Z. Y. Sun, *J. Mater. Chem. A* **2017**, *5*, 7257 – 7284; e) Y. P. Wang, C. W. Zhang, W. X. Ji, R. W. Zhang, P. Li, P. J. Wang, M. J. Ren, X. L. Chen, M. Yuan, *J. Phys. D* **2016**, *49*, 055305; f) J. Zhao, Z. H. Qi, Y. Xu, J. Dai, X. C. Zeng, W. L. Guo, J. Ma, *WIREs Comput. Mol. Sci.* **2019**, *9*, e1387.

[10] X. H. Niu, Y. H. Li, Q. H. Zhou, H. B. Shu, J. L. Wang, *ACS Appl. Mater. Interfaces* **2017**, *9*, 42856 – 42861.

[11] H. L. Chia, N. M. Latiff, R. Gusmao, Z. Sofer, M. Pumera, *Chem. Eur. J.* **2019**, *25*, 2242 – 2249.

[12] X. W. Zhang, X. J. Yan, Z. R. Zhou, F. F. Yang, Z. Y. Wu, H. B. Sun, W. X. Liang, A. X. Song, V. Lallemand-Breitenbach, M. Jeanne, Q. Y. Zhang, H. Y. Yang, Q. H. Huang, G. B. Zhou, J. H. Tong, Y. Zhang, J. H. Wu, H. Y. Hu, H. de The, S. J. Chen, Z. Chen, *Science* **2010**, *328*, 240 – 243.

[13] a) L. A. R. Group, *N. Engl. J. Med.* **2014**, *370*, 1866; b) M. Jeanne, V. Lallemand-Breitenbach, O. Ferhi, M. Koken, M. Le Bras, S. Duffort, L. Peres, C. Berthier, H. Soilihi, B. Raught, H. de The, *Cancer Cell* **2010**, *18*, 88 – 98.

[14] V. Nicolosi, M. Chhowalla, M. G. Kanatzidis, M. S. Strano, J. N. Coleman, *Science* **2013**, *340*, 1226419.

[15] J. M. Calleja, J. S. Lannin, M. Cardona, E. Schonher, *Bull. Am. Phys. Soc.* **1974**, *19*, 227.

[16] J. S. Lannin, *Phys. Rev. B* **1977**, *15*, 3863 – 3871.

[17] R. Gusmão, Z. Sofer, D. Bouša, M. Pumera, *Angew. Chem. Int. Ed.* **2017**, *56*, 14417 – 14422; *Angew. Chem.* **2017**, *129*, 14609 – 14614.

[18] a) R. Gusmão, Z. Sofer, D. Bousa, M. Pumera, *Angew. Chem. Int. Ed.* **2017**, *56*, 14417 – 14422; *Angew. Chem.* **2017**, *129*, 14609 – 14614; b) A. Ambrosi, M. Pumera, *Chem. Soc. Rev.* **2018**, *47*, 7213 – 7224.

[19] L. L. Guo, H. Chen, N. Y. He, Y. Deng, *Chin. Chem. Lett.* **2018**, *29*, 1829 – 1833.

[20] S. J. Gilliam, C. N. Merrow, S. J. Kirkby, J. O. Jensen, D. Zeroka, A. Banerjee, *J. Solid State Chem.* **2003**, *173*, 54 – 58.

[21] a) A. Nel, T. Xia, L. Madler, N. Li, *Science* **2006**, *311*, 622 – 627; b) A. Nel, *Science* **2005**, *308*, 804 – 806.

[22] K. M. Andersen, L. Madsen, S. Prag, A. H. Johnsen, C. A. Semple, K. B. Hendil, R. Hartmann-Petersen, *J. Biol. Chem.* **2009**, *284*, 15246 – 15254.

[23] J. E. Wagner, D. Collins, S. Fuller, L. R. Schain, A. E. Berson, C. Almici, M. A. Hall, K. E. Chen, T. B. Okarma, J. S. Lebkowski, *Blood* **1995**, *86*, 512 – 523.

[24] a) S. D. Freeman, S. Kelm, E. K. Barber, P. R. Crocker, *Blood* **1995**, *85*, 2005 – 2012; b) K. Naito, A. Takeshita, K. Shigeno, S. Nakamura, S. Fujisawa, K. Shinjo, H. Yoshida, K. Ohnishi, M. Mori, S. Terakawa, R. Ohno, *Leukemia* **2000**, *14*, 1436 – 1443.

[25] a) J. Shao, H. Xie, H. Huang, Z. Li, Z. Sun, Y. Xu, Q. Xiao, X. F. Yu, Y. Zhao, H. Zhang, H. Wang, P. K. Chu, *Nat. Commun.* **2016**, *7*, 12967; b) X. D. Zhang, J. Chen, Y. Min, G. B. Park, X. Shen, S. S. Song, Y. M. Sun, H. Wang, W. Long, J. P. Xie, K. Gao, L. F. Zhang, S. J. Fan, F. Y. Fan, U. Jeong, *Adv. Funct. Mater.* **2014**, *24*, 1718 – 1729.

Manuscript received: October 26, 2019
Accepted manuscript online: December 31, 2019
Version of record online: February 3, 2020